Exchange Couplings and Magneto-Structural Correlations of Trinuclear MII-UIV-MII (MII=Co, Ni, Cu) Complexes

Lotfi Belkhiri, Rémi Maurice, Boris Le Guennic, Abdou Boucekkine, Michel Ephritikhine

Exchange Couplings and Magneto-Structural Correlations of Trinuclear M^{II}-U^{IV}-M^{II} (M^{II} = Co, Ni, Cu) Complexes.

Lotfi Belkhiri,[a,b*] Rémi Maurice,[c] Boris Le Guennic,[c] Abdou Boucekkine,[c*] and Michel Ephritikhine[d]

[a] Laboratoire de Physique Mathématique et Subatomique LPMS, Département de Chimie, Université des Frères Mentouri Constantine 1, 25017, Algeria.
[b] Centre de Recherche en Sciences Pharmaceutiques CRSP, Ali Mendjeli, 25000 Constantine, Algeria.
[c] Univ Rennes, CNRS, ISCR (Institut des Sciences Chimiques de Rennes) - UMR 6226, 35000 Rennes, France.
[d] NIMBE, CEA, CNRS, Université Paris-Saclay, CEA Saclay, 91191 Gif-sur-Yvette, France.

Abstract:

The magnetic properties of the trinuclear Schiff base complexes M_2UL^7 (M^{II} = Co, Ni, Cu; L^7 = *N,N'*-bis(3-hydroxysalicylidene)-2,2-dimethyl-1,3-propanediamine), exhibiting the $[M(\mu\text{-}O)_2]_2U$ core structure (3d–5f–3d subsystem), have been investigated theoretically using scalar relativistic ZORA/DFT computations combined with the broken symmetry (BS) approach. The calculated coupling constants J_{MU} between the adjacent M1–U and M2–U agree with the observed ferromagnetic (Ferro) character observed in the case of the Cu_2UL^7 complex, the antiferromagnetic (AF) character of the Ni_2UL^7 one is consistent with the experimentally observed AF behaviour for Co_2UL^7. The structural parameters, in particular the M–U distances and the M–O_b–U angles, as well as the electronic factors driving the superexchange couplings are discussed. The bond orders and the magnetic molecular orbital analyses reveal that the U(5f) covalent contribution to the bonding within the M–O–U coordination is more important in the Co_2UL^7 and Ni_2UL^7 complexes than in the Cu_2UL^7 congener, thus favouring AF coupling between the transition metal and the uranium magnetic centers, in the first complexes. The analyses are supported by the study of the mixed $ZnMUL^7$ and M_2ThL^7 systems, where the Co^{II} ($3d^7$) and Ni^{II} ($3d^8$) paramagnetic ions are replaced by the diamagnetic Zn^{II}($3d^{10}$) one, whereas in the second complex, the U^{IV}($5f^2$) paramagnetic center is replaced by the diamagnetic Th^{IV}($5f^0$) one. The Natural Populations Analyses confirm the crucial role of spin delocalization that is at work in favour of the AF vs. Ferro magnetic character of the M–U–M (M = Ni, Co) and Cu–U–Cu coordination, respectively.

Keywords: 3d-5f-3d complexes; magneto-structural correlations; super-exchange; DFT, Broken Symmetry.

Corresponding Authors:

*Email (A. Boucekkine): abdou.boucekkine@univ-rennes.fr
*Email (L. Belkhiri): lotfi.belkhiri@umc.edu.dz

Introduction:

Over the last two decades, an increasing number of heteropolymetallic 3d–4f and 3d-5f mixed complexes have aroused intense attention, both from experimental and theoretical sides, due to their opening new perspectives in the design of molecular magnets (SMMs) [1-9], and their exceptional promising applications such as ultra-high-density data storage, spintronic, and quantum information processing (QIP) [10]. Besides its fundamental aspect, the understanding of the nature of metal-ligand bonding and metal–metal 3d–4f/5f electronic interactions, in the lanthanide and actinide coordination compounds, is crucial in the design of novel magnetic materials [11]. In particular, examples of trinuclear M^{II}–U^{IV}–M^{II} complexes have been reported recently to show unambiguous magnetic M–U coupling between the metal spin carriers [12-15].

The exchange coupling between 3d and 5f ions has been studied to develop an accurate theoretical description of an effective magnetic interaction [16-21]. Notably, the larger spatial extent of the actinide 5f orbitals relative to the 4f ones [22-24] could favor stronger exchange couplings with 3d transition metals, resulting in larger antiferromagnetic (AF) or ferromagnetic (Ferro) couplings. Therefore, efforts in this area have been devoted to synthesizing and characterizing polynuclear uranium systems, where a successful strategy for promoting electronic interactions between 5f spin centers was to use covalently linked bridging ligands [25−30]. However, such mixed 3d-5f polymetallic compounds remain rare, and to date, there are only a few X-ray-determined structures for which a magnetic superexchange coupling constant has been measured, as was recently reviewed [1,3,10]. Furthermore, quantifying the coupling constant between 5f ion pairs is still challenging at both the experimental and theoretical levels [8,11,23,24].

Early in the 2000s, Ephritikhine and co-workers [31−34] synthesized an interesting class of trinuclear Schiff-based $M^{II}_2An^{IV}L^i$ (M = Zn, Cu; An = Th, U; L = Schiff base; i = 1-9) assemblies exhibiting double oxo-bridged $[Cu(\mu\text{-}O)]_2U$ core with different magnetic exchange M^{II}–U^{IV} interactions. Indeed, as reported by the authors [33,34], it was found that the shift from AF character to Ferro observed experimentally for the Cu^{II}–U^{IV} coupling, depends strongly on the diimino backbones (L^i). Scalar relativistic ZORA/B3LYP investigations of their magneto-structural properties, indicate a moderate magnetic exchange coupling constant J_{CuU}, with lower and upper bounds $-2.4 < J < +7.0$ cm^{-1} [35], which is in good agreement with the available experimental fitted values ($-3.6 < J_{min} < +5.2$ cm^{-1}) [24]. Moreover, this AF to Ferro

shift, when passing from the L^1 to L^9 diimino-backbone, correlates with the decrease of the uranium orbitals weight (covalency) in the magnetic $[Cu(\mu\text{-}O)]_2U$ core, limiting the superexchange responsible for the AF Cu^{II}–U^{IV} character [35].

A few years afterward, S.A. Kozimor *et al*. [36,37] reported the magnetic properties of the trinuclear pyrazolate-chloro-bridged $M^{II}(\mu\text{-}Cl)U^{IV}$ (M^{II} = Co, Ni, Cu, and Zn) complexes of the formula (cyclam)$M[(\mu\text{-}Cl)U^{IV}(Me_2Pz)_4]_2$ (cyclam = 1,4,8,11-tetraazacyclotetradecane; Me_2Pz^- = 3,5-dimethylpyrazolate). Strong Ferro coupling ($15\ cm^{-1} < J_{U-M} < 48\ cm^{-1}$) is observed for the Co^{II}-containing species (−2J convention). DFT calculations performed on the CoU_2 and Ni_2U model clusters consistently revealed a weaker ferromagnetic Ni–U coupling constant ($2.8\ cm^{-1} < J < 19\ cm^{-1}$) than for the Co–U congener [37].

More recently, UO_2^+–M^{2+} interactions provide a very convenient route for the controlled assembly of oxo-bridged 3d–5f complexes and promote the cation–cation interactions between the UO_2^+group and the 3d cations. Indeed, as reported by Mazzanti and co-workers [12–15], these hetero-polymetallic complexes which exhibit a M^{II}–O=U^V=O–M^{II} (M^{II} = Mn, Fe, Co, Ni) linear oxo-core, are of great interest for the design of molecules presenting slow magnetic relaxation of a purely molecular origin and described as single-molecule magnets (SMMs), and have been put forward as an effect of the 3d spin ion on the magnetic properties [2, 12–15]. Indeed, for the trimers in which the 3d metal adopts an octahedral geometry, the value of the energy barrier is directly correlated to the spin ground state, and it decreases along the high spin (Mn > Fe > Ni) series (Mn^{II}: S = 5/2; Fe^{II}: S = 2; and Ni^{II}: S = 1). Moreover, the low value of χT observed at ∼2 K is due to the strong AF interactions in UO_2^+–Mn and a weaker AF interaction between U^V centers [15]. Moreover, broken symmetry DFT calculations in the case of the Mn–O=U=O–Mn core species have been carried out to estimate the isotropic coupling constants of the adjacent Mn^{II}–U^V and next-adjacent Mn^{II}---Mn^{II} exchange interactions, leading to $J_{12} = J_{23} = 49.7\ cm^{-1}$ and $J_{13} = 0.5\ cm^{-1}$, respectively [12].

Along with the continuous improvement of our understanding of how the properties of the transition metal (3d) can modulate the nature of such superexchange 3d–5f interactions, we extend our computational investigation of the magnetostructural correlation to the $[\{L^7M^{II}\}_2U^{IV}]$ (M^{II} = Co, Ni) analogous, associated to the Schiff base L^7 (*N,N'*-bis(3-hydroxysalicylidene)-2,2-dimethyl-1,3-propanediamine}) [32], and for which no systematic theoretical study has been carried out up to now, to our knowledge. In this $[\{L^7M^{II}\}_2U^{IV}]$ systems, hereafter called M_2UL (M = Co, Ni), the structures are built up by two LM units bound to the central uranium(IV) ion by two pairs of oxygen atoms, leading to the $[M(\mu\text{–}O_b)_2]_2U$

cores, as shown on Figure 1. Note that the corresponding O–U–O bond angles are either nearly linear (180°) or orthogonal (90° for *trans* U–O bonds).

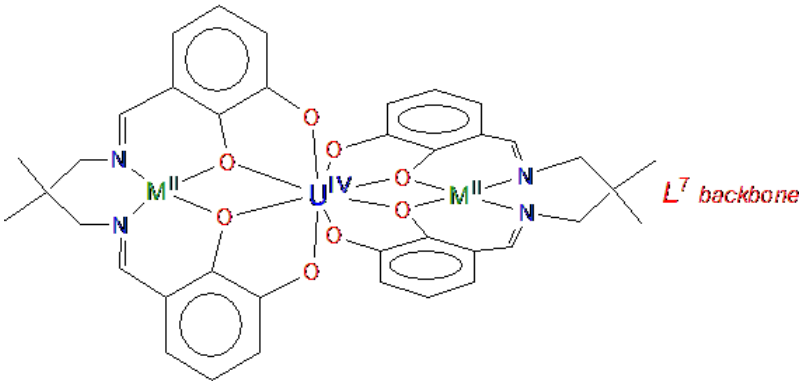

Figure 1: Molecular structure of the M_2UL (M = Co, Ni) complexes.

Experimentally, the observed magnetic behavior by susceptibility measurements of the Co_2UL, Ni_2UL, and Cu_2UL isostructural complexes was compared with that of the Zn_2UL derivative [31,32], in which the paramagnetic 3d ion was replaced with the diamagnetic Zn ($3d^{10}$) ion. Application of the subtraction method of Zn_2UL data from the M_2UL (M = Co, Ni, Cu) one, gave $\Delta\chi_M T$ vs T plots that show weak AF coupling between the central U^{IV} ion and the paramagnetic transition Ni^{II} metal ions, in contrast to the Ferro coupling exhibited by the Cu_2UL species [31,32]. As noted by the authors, the continuous increase in the $\Delta\chi_M T$ vs T curve, even well above 100 K, cannot be attributed to the local zero-field splittings of the Ni^{II} ions (single-ion anisotropies), which thus drove them to the conclusion that isotropic couplings were at play. Note that by subtracting the angular momentum of the U^{IV} ion, it is assumed that the $\Delta\chi_M T$ vs T curve is the result of the local zero-field splittings and of rests of interactions between the paramagnetic ions. Further assuming larger nearest-neighbor interactions than next-nearest neighbor ones, they concluded for AF coupling between the Ni^{II} metal ions and the U^{IV} one. Despite having observed the exact same behavior in the Co_2UL case, the authors did not concluded on the coupling between the Co^{II} ions and the U^{IV} one, since the Co^{II} centers themselves could be the subject of orbital momentum. In this case, we thus aim at predicting the nature of the coupling between the Co^{II} ions and the U^{IV} one. Recently, the exchange coupling in two dicobalt(II) complexes i.e., $[Co_2Cl_6]^{2-}$ and $[Co_2(L)_2(acac)_2(H_2O)]$, was theoretically investigated by simulating the χT curve based on various assumptions of the underlying model Hamiltonian, that included isotropic, zero-field splitting and anisotropic exchange [38]. It was clearly seen that the combination of Ferro coupling with large zero-field

splitting may lead to a maximum of the χT curve at low temperature, and continuous increase of χT can only be explained if an AF coupling occurs.

Overall, the present study aims to get more clear-cut insights into the electronic structure and magnetic properties of the mixed 3d–5f M_2UL (M = Co, Ni, Cu, Zn) complexes under consideration. The dependence of the exchange coupling on the electronic and structural properties namely the M_2O_4U core geometry i.e., the M^{II}–U^{IV} distances and the M–O_b–U angle will be investigated thoroughly. It is hoped that this computational study will permit the rationalization of the observed differentiation in magnetic superexchange M^{II}–U^{IV}–M^{II} (M = Co, Ni, Cu) interactions, and the role of 3d-metal electron spins properties could be brought to light.

Methods

a. Computational Details

All calculations were performed with the Amsterdam Density Functional (ADF) program, a part of the Amsterdam Molecular Simulation package (AMS2021.107 release) [39, 40]. Scalar relativistic corrections have been introduced via the zeroth-order regular approximation (ZORA) [41, 42]. In all cases, the starting molecular structures for the geometry optimizations are derived from the structures of the M_2UL (M^{II} = Co^{II}, Ni^{II}) complexes in the reported X-ray data [32-34]. As successfully used previously [35], the geometry optimization of the M_2UL complexes was carried out by fixing the $[M(\mu–O_b)_2]_2U$ core as it is in the X-ray structure. However, we noted that the full geometry optimization of the whole complex including the M_2O_4U core, leads to an overestimation of the exchange coupling J constant, and even a slight distortion of the core M_2O_4U geometry from the X-ray structure affects drastically the magnetic properties [35]. Notably, it was observed in the case of the dichromium(III) systems exhibiting dihydroxo $Cr_2(\mu\text{-}OH)_2$ core [43,44], and in dioxo-diuranium systems exhibiting the diamond $U_2(\mu\text{-}O)_2$ core [26], replacing the DFT core geometry by the X-ray one, matches better with magnetic data.

The DFT geometry optimizations of the High Spin (HS) states, which have been carried out using the BP86 functional of Becke and Perdew [45, 46], employed triple-ζ-plus polarization (TZP) all-electron Slater type orbitals (STO) basis sets. Such a ZORA/BP86/TZP procedure, which has been successfully used in our previous related works [17, 25-27], and in several other theoretical studies [47, 48], has shown to reproduce the experimental geometries of f-element compounds with a satisfying accuracy. Moreover, the computation of the *J*

exchange coupling constant has been done using the standard B3LYP hybrid functional [49, 50] as recommended in previous studies [51]. The B3LYP HS energies were obtained by performing a single-point calculation using the BP86 optimized geometries. Then, the MOs of the HS structures were used as starting guesses, to compute the BS states [52,53] by means of the spin-flip recipe available in the AMS/ADF program [39].

Molecular structure drawings spin densities and molecular orbital plots were generated using the ADF-GUI auxiliary program [39]. Finally, in the calculation, the ADF integration accuracy parameter, i.e. the grid numerical quality was set as high as 10^{-6} eV (numerical accuracy keyword "good"). We remind that the ADF program computes Total Bonding Energies (TBE) and not total energies [40], though this as no impact on the energy differences of interest for the sake of computing magnetic exchange coupling constants.

b. Evaluation of the exchange coupling

The magnetic interaction between two atomic spins is usually described by the Heisenberg-Dirac-van Vleck (HDvV) Hamiltonian, as given by ($-J$ convention):

$$\hat{H} = -J_{AB}\hat{S}_A \cdot \hat{S}_B \qquad (1)$$

where J_{AB} is the coupling constant between the A and B magnetic sites and $\hat{S}_A$ and $\hat{S}_B$ are the local spin operators (the vector notations are omitted as commonly done in the literature). A positive sign of the coupling constant J indicates a Ferro interaction (parallel alignment of spins), whereas a negative sign indicates an AF interaction (anti-parallel alignment of spins). As reported in previous studies on polynuclear transition metal complexes [17,54], the Heisenberg Hamiltonian equation (1) can be extended to calculate the exchange coupling constants at play in polynuclear complexes by summing over all the independent pairs of active magnetic centers.

For the trinuclear M_2UL (M = Co, Ni) complexes considered here, the spin coupling model includes exchange interactions between adjacent metal centers, J_{12} and J_{23}, and the coupling between the terminal transition metal centers, J_{13}, as shown on scheme 1.

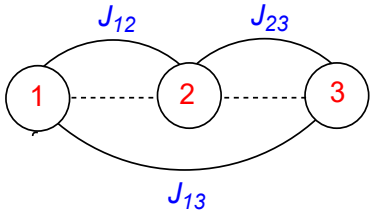

Scheme 1: the three exchange coupling constants at play in trinuclear complexes

The resulting Hamiltonian, obtained by summing all the bicentric terms, is given by equation 2:

$$\hat{H} = -J_{12}\hat{S}_1 \cdot \hat{S}_2 - J_{23}\hat{S}_2 \cdot \hat{S}_3 - J_{13}\hat{S}_1 \cdot \hat{S}_3 \qquad (2)$$

Considering $S_1 = S_3 = 1$ for the Ni^{II} (d^8) and $S_1 = S_3 = \frac{3}{2}$ for the Co^{II} (d^7) metal centers and $S_2 = 1$ for the U^{IV} ($5f^2$) center, four non-equivalent spin configurations obtained by parallel and/or anti-parallel alignments of the adjacent spins are obtained (see Scheme 2), with the HS state for the two Co_2U and Ni_2U systems having the $M_S = 4$ and 3 values, respectively. Note that we checked (*vide infra*) that the transition metal exhibits the high spin state in the ligand field experienced in the trinuclear complexes. The BS solutions are obtained by flipping the spins on centers 1 and 3, which leads to $M_S = -1$ for M = Ni and $M_S = -2$ for M = Co, respectively, while the BS1 and BS2 solutions are obtained by flipping the spin on centers 1 or 3, which leads in any case to $M_S = 1$ [17,54].

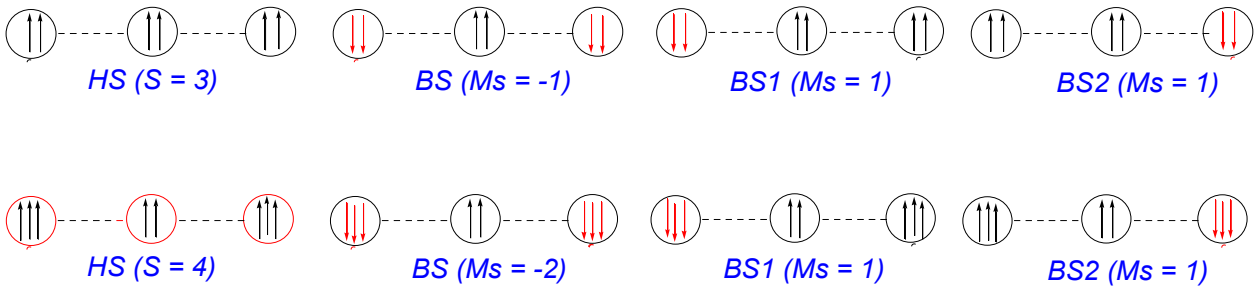

Scheme 2: the spin configurations of interest (top line: Ni centers; bottom line: Co centers)

Using equation 2 and scheme 2, the relative energies of these four configurations can be explicitly written in terms of the coupling constants J_{12}, J_{23}, and J_{13}.

The zero of energy is equal to the mean energy of the four computed configurations [21], as follows:

$$E_o = \frac{E_{HS}+E_{BS}+E_{BS1}+E_{BS2}}{4} \qquad (3)$$

Therefore, the energies of the four HS, BS1, BS2 and BS states are expressed for the two Ni_2U and Co_2U systems as:

Case of Ni-U-Ni, d^2-f^2-d^2:

$S1 = S2 = S3 = 1$

- HS: αα-αα-αα

$E_{HS} = E_0 - J_{12} - J_{23} - J_{13}$

- BS: ββ-αα-ββ

$E_{BS} = E_0 + J_{12} - J_{23} + J_{13}$

- BS1: ββ-αα-αα

$E_{BS1} = E_0 - J_{12} + J_{23} + J_{13}$

- BS2: αα-αα-ββ

$E_{BS2} = E_0 + J_{12} + J_{23} - J_{13}$

By differentiating, one leads to:

$E_{HS} - E_{BS} = -2J_{12} - 2J_{13}$ (4)

$E_{HS} - E_{BS1} = -2J_{23} - 2J_{13}$ (5)

$E_{HS} - E_{BS2} = -2J_{12} - 2J_{23}$ (6)

$E_{BS} - E_{BS1} = 2J_{12} - 2J_{23}$ (7)

$E_{BS} - E_{BS2} = -2J_{23} + 2J_{13}$ (8)

Then, (4) – (6) leads to:

$(E_{HS} - E_{BS}) - (E_{HS} - E_{BS2}) = -2J_{13} + 2J_{23}$

(4) + (5) – (6) then gives:

$(E_{HS} - E_{BS}) + (E_{HS} - E_{BS1}) - (E_{HS} - E_{BS2}) = -4J_{13}$

Thus,

$$\mathbf{J_{13} = -[E_{HS} - E_{BS} - E_{BS1} + E_{BS2}]/4} \quad (9)$$

J_{12} and J_{23} are finally obtained by:

$$\mathbf{J_{12} = -\tfrac{1}{2}[(E_{HS} - E_{BS}) + 2J_{13}]} \quad (10)$$

$$\mathbf{J_{23} = = -\tfrac{1}{2}[(E_{HS} - E_{BS1}) + 2J_{13}]} \quad (11)$$

Case of Co-U-Co d^3-f^2-d^3:

$S1 = S3 = 3/2, S2 = 1$

$E_0 = ¼ (E_{aaa} + E_{baa} + E_{bab} + E_{aab})$

- HS: ααα-αα-ααα:

$E_{HS} = E_0 - 3/2J_{12} - 3/2J_{23} - 9/4J_{13}$

- BS: βββ-αα-βββ:

$E_{BS} = E_0 + 3/2J_{12} + 3/2J_{23} - 9/4J_{13}$

- BS1: βββ-αα-ααα:

$E_{BS1} = E_0 + 3/2J_{12} - 3/2J_{23} + 9/4J_{13}$

- BS2: ααα-αα-βββ:

$E_{BS2} = E_0 - 3/2J_{12} + 3/2J_{23} + 9/4J_{13}$

$E_{HS} + E_{BS1} = 2E_0 - 3J_{23}$ (12)

$E_{HS} + E_{BS} = 2E_0 - 9/2J_{13}$ (13)

$E_{BS1} + E_{BS} = 2E_0 + 3J_{12}$ (14)

$E_{BS1} + E_{BS2} = 2E_0 + 9/2J_{13}$ (15)

From (13) – (15):

$E_{HS} + E_{BS} - E_{BS1} - E_{BS2} = -9J_{13}$

$\mathbf{J_{13} = -1/9(E_{HS} + E_{BS} - E_{BS1} - E_{BS2})}$ (16)

$E_{HS} - E_{BS1} = -3J_{12} - 9/2J_{13}$ (17)

$E_{HS} - E_{BS} = -3J_{12} - 3J_{23}$ (18)

$E_{BS1} - E_{BS} = -3J_{23} + 9/2J_{13}$ (19)

From (14):

$\mathbf{J_{12} = -1/3\ (E_{HS} - E_{BS1} + 9/2\ J_{13})}$ (20)

From (19):

$\mathbf{J_{23} = -1/3\ (E_{BS1} - E_{BS} - 9/2\ J_{13})}$ (21)

For bicentric spin centers, the Yamaguchi equation [55-57] which is reported to be valid over the full range of coupling strengths, from the weak to the strong overlap limit [17], is used as follows, where $<S^2>$ is the mean value of the squared spin operator:

$$J_{AB} = \frac{E_{BS} - E_{HS}}{<S^2>_{HS} - <S^2>_{BS}} \quad (22)$$

One can note that in our case (weak-coupling scheme), no significant deviation is expected from the Ising coupling scheme.

For the computation of the BS, BS1, and BS2 energies, a single-point calculation using the molecular orbitals (MOs) of the HS structure has been used as a starting guess, changing the spin on the corresponding metal center in each case [35]. It must be kept in mind that the energy differences between the different multiplets HS, BS, BS1, and BS2 states, is often

smaller than ~0.5 kcal/mol (*i.e.* ~170 cm^{-1}) [58] so that a very good accuracy of the evaluation of the coupling constant *J*, must be insured to avoid numerical round-up errors.

Furthermore for the mixed ZnUM (M = Co, Ni) model complexes, exhibiting only two magnetic centers M^{II}–U^{IV} for two electronic configurations i.e., $3d^7$–$5f^2$ and $3d^8$–$5f^2$, respectively, the formula of Yamaguchi et al. (Eq. 22) can be used for the evaluation of the coupling constant *J*. Note that the "diamagnetic" approach was successfully used in the cases of the mixed trinuclear Ni^{II}–Gd^{III}–Ni^{II} systems, by replacing one of the Ni^{II} ions by Zn^{II} [54]. Finally, for the MThM (M = Co, Ni) congeners, exhibiting two magnetic M^{II}---M^{II} centers and exhibiting two electronic configurations i.e., $3d^7$–$3d^7$ and $3d^8$–$3d^8$, the same Yamaguchi equation is used.

Results and Discussion

a. Geometry optimizations

It is known that the coordination complexes of Co ($3d^7$) or Ni ($3d^8$), could exhibit either a high spin (HS) or a low spin state (LS), depending on ligand field strength [12,13]. Thus, in order to fix the spin state of the transition metal in the 3d-5f-3d systems we carried out preliminary calculations considering monometallic MLpy (M = Co, Ni) model complexes. We found that the HS state is the most stable one in both cases.

We started the study of the trinuclear M_2UL (M^{II} = Co, Ni) systems by optimizing the available X-ray structures [31-33]. For the Zn_2AnL (M^{II} = Co, Ni; An^{IV}= Th, U) derivatives, experimental structures are also available so we extracted their initial molecular geometries for optimization from the X-ray data of their ZnUML models. The full geometry optimization that we previously carried out on Cu_2UL^i (I = 1-9) systems [35], showed that small deviations between the X-ray and the fully optimized structures (*vide supra*) could be of tremendous importance for the magnetic property under consideration. Consequently, for the analysis of the magnetic properties of the trinuclear M_2UL species, we considered the M_2O_4U core X-ray geometry fixed.

First, let us consider the M_2AnL (M^{II} = Ni, Co, Zn; An^{IV} = Th, U) structures obtained from the ZORA/BP86/TZP geometry optimizations, displayed on Figure 2 along with the most relevant structural parameters of the magnetic core depicted on Figure 3.

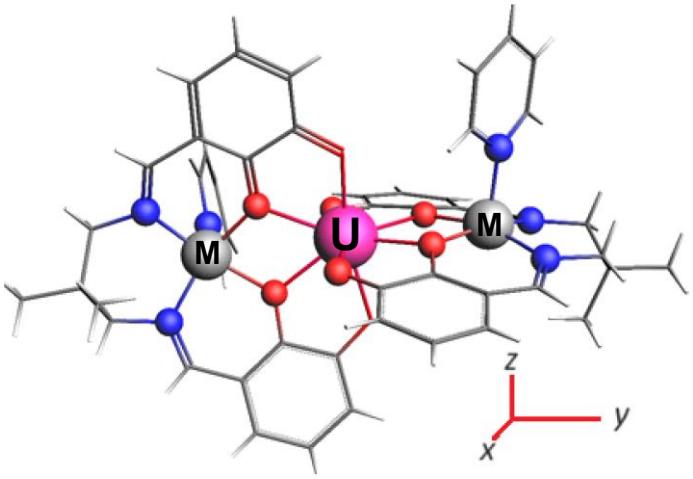

(a) MUM

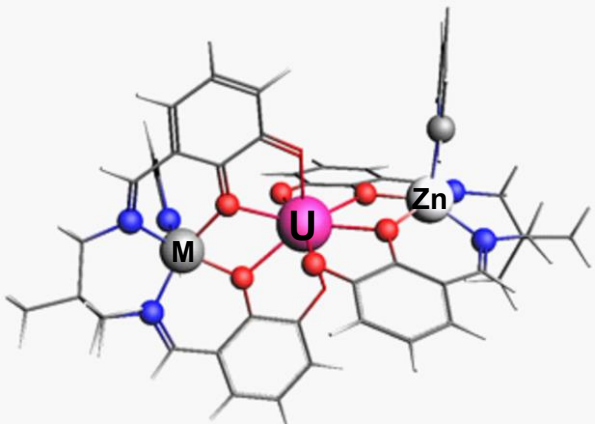

(b) MUZn

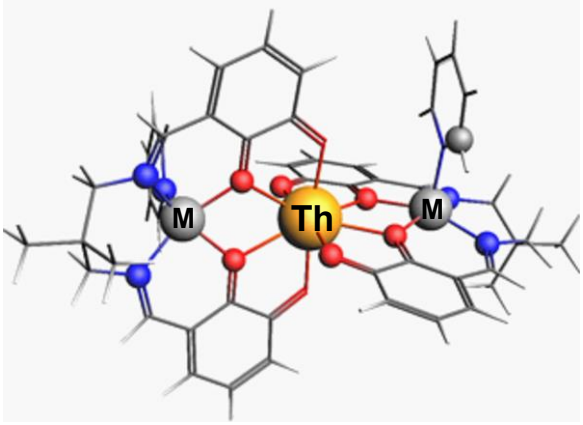

(c) MThM

Figure 2: Optimized molecular structures of the MUM (M^{II} = Co, Ni) X-ray fixed core complexes, their (b) MUZn and (c) MThM model systems (Pink = uranium; yellow = thorium; grey = cobalt and nickel; light grey = Zinc; red = oxygen; blue = nitrogen).

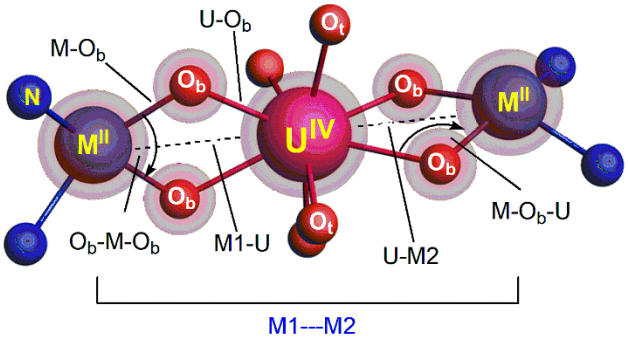

Figure 3: geometrical parameters of the $M_2(\mu\text{-}O_b)_4U$ core

In Table 1, we report the two optimized metal–uranium sides of M1–U/U–M2 distances and the average <M–O_b> and <U–O_b> bond distances (Å) as well as the interatomic M–M distance. The average <M1–O_b–U> and <M2–O_b–U> bond angles (°) for both sides are also reported as well as the M–U–M angle for the M_2UL (M^{II} = Co, Ni) complexes in their HS state.

Table 1: Relevant X-ray (<av.>) bond distances (Å) and angles (°) for the fixed core M_2UL (M^{II} = Co, Ni, Cu, Zn) complexes in their HS states (S = 4, 3, 2, and 1, respectively). See Figure 3 for the definition of the geometrical parameters of the fixed core.

M_2UL X-ray fc	M–U (Å)	<M–O_b> (Å)	<U–O_b> (Å)	M–M (Å)	<M–O_b–U> (°)	M–U–M (°)
CuUCu (S =2) [a]	3.634/3.648	1.918/1.949	2.433/2.459	7.279	111.5/112.3	177.27
av.	<3.641>	<1.933>	<2.446>			
NiUNi (S = 3)	3.633/3.652	1.976/1.988	2.421/2.433	7.269	110.6/111.7	172.28
av.	<3.642>	<1.982>	<2.427>			
CoUCo (S = 4)	3.666/3.693	1.993/2.002	2.453/2.458	7.340	110.4/111.3	171.84
av.	<3.679>	<1.997>	<2.455>			
ZnUZn (S = 1)[b]	3.682/3.718	2.217/2.451	2.431/2.451	7.339	110.4/112.3	170.93
av.	<3.700>	<2.310>	<2.441>			

[a] [35], [b] [32]

One can note that the M–U bond distances are slightly smaller for the Ni_2UL species than for the Co_2UL congener (in av. 3.642 vs. 3.679 Å). The oxo-bridge <M–O_b> and <U–O_b> bonds are also found shorter (in av. 1.982 vs. 1.997 and 2.427 vs. 2.455). For the M_2UL (M = Co, Ni) species, described as AF systems, the <M–O_b–U> bond angles are computed to be smaller comparatively to the Cu_2UL Ferro congener.

Finally, it appears that the main significant structural differences regarding the M(μ–O_b)$_2$U magnetic core, when changing the transition metal, are the M–O_b–U angles or the M–U distance variations.

b. Electronic structure analyses.

To study the electronic structures and the nature of the metal-ligand bonding in the M_2UL (M = Co, Ni) complexes, natural population analyses (NPA) [59], Mayer [60], and Nalewajski-Mrozek (NM) [61, 62] bond order analyses were performed at the optimized ZORA/BP86/TZP equilibrium geometries with the M_2O_4U core fixed (See Figure 3). The B3LYP computed net natural atomic charges (q), Mayer, and NM bond orders are given in Table 2.

Table 2: ZORA/B3LYP/TZP NPA atomic spin density (ρ_α–ρ_β) and net charges (q), Mayer and NM average <M–O_b> and <U–O_b> bond orders of the MUM complexes in their HS and BS states.

M2ULpy2		NPA M1/U/M2		Bond Order <M–O_b>		Bond Order <U–O_b>	
		ρ_α–ρ_β	q	Mayer	NM	Mayer	NM
CuUCu (S = 2)[a]	HS	0.64/2.04/0.61	1.39/1.72/1.43	0.359	0.834	0.162	1.132
	BS	–0.63/2.03/–0.60	1.38/1.73/1.39	0.358	0.836	0.169	1.149
NiUNi (S = 3)	HS	1.61/2.03/1.61	1.42/1.69/1.43	0.424	0.924	0.198	1.156
	BS	–1.41/2.03/–1.50	1.42/1.69/1.43	0.422	0.978	0.198	1.162
CoUCo (S = 4)	HS	2.62/2.04/2.62	1.47/1.73/1.47	0.449	1.054	0.216	1.173
	BS	–1.90/2.03/–1.90	1.17/1.73/1.18	0.447	1.296	0.222	1.184

[a] [35]

The results of Table 2 show that the atomic spin densities of the uranium atom are close to or slightly larger than the number of unpaired electrons of the U(IV) ion, i.e., 2, whereas the values for the copper ($3d^9$), nickel ($3d^8$), and cobalt ($3d^7$) atoms are significantly lower than their number of unpaired electrons, namely 1, 2, and 3, respectively. Notably, the spin densities of the metal ions M^{II}, are computed significantly smaller for the cases of MUM (Ni, Co) systems, when passing from the HS to the BS states, especially for the Co_2UL, while the values remain constant in the cases of the CuUCu congener. These spin densities are indicative of the spin delocalization (oxidation) occurring for the transition metal ions, and will be discussed in-depth below. Moreover, the computed NPA charges on the uranium atom are *ca*. +1.71, which is much smaller than the formal value of +4 in U(IV), revealing the ligand-to-metal donation.

Interestingly, the NM <M–O_b> and <U–O_b> HS bond orders, which account for covalent and ionic interactions, are computed significantly greater for the AF Co_2U and Ni_2U species (0.924 and 1.054 for <M–O_b> and 1.156 and 1.173 for <U–O_b>) than for the Ferro Cu_2U congener (respectively 0.834 and 1.132). Moreover, the Mayer bond orders are computed higher for the cobalt and nickel complexes than for the copper one (Table 2). These results correlate with the higher covalency in M–O_b–U (M = Co, Ni) bonding than in Cu system, and will be assessed in-depth by orbital analysis bellow.

As previously observed in oxo-bridged systems, the metal-oxygen M–O_b covalent bonds, could promote "electronic communication" that favors metal-metal super-exchange couplings and

the AF character not only in 3d–5f mixed systems exhibiting oxo-bridged ligands [4,12-14,24,35], but also in polymetallic clusters with M–O–M frameworks as nicely reviewed by Dossing et al. [63,64]. Indeed, the resulting M–O–M superexchange coupling in polymetallic systems can occur through 3d–2p–3d overlap between metal centers. Moreover, as reported by the review [63], theoretical calculations of the magneto-structural properties using DFT in combination with the BS approach, when the Cr–O distances have been elongated or compressed up to 0.02 Å, revealed that the superexchange coupling is strongly sensitive to change in the oxo-bridge coordination from linear M–O–M to bend structures [63].

Traditionally, the theoretical orbital interpretation of superexchange interactions, has been developed by the Hay-Thibeault-Hoffmann model [65], reporting that the bridging overlap interactions between the ligand atomic orbitals and the metal d ones determine the sign and magnitude of the exchange interaction. Recently, it is noteworthy that the magnetic exchange of lanthanides and actinides elements with 3d metals has been reported by McAdams et al. [10], highlighting that the enhanced covalency of actinides in comparison to the more core-like lanthanides, favors magnetic superexchange with other 3d metal ions through oxo-ligands.

It appears that more pronounced covalent factors of the M–O_b and U–O_b bonds in the Ni_2U and Co_2U, are playing significant role in promoting M–U–M superexchange AF interactions.

The comparative frontier MO diagrams of the M_2UL (M = Cu, Ni, Co) systems in their HS (S = 2, 3, 4) states are shown on Figure 4. Note that due to the *spin-unrestricted* formalism, Kohn-Sham orbitals are formally called ‘KS spin orbitals’ in the caption, which does not mean at all that the SOC (spin orbit coupling) is accounted for in our calculations (in practice, two sets of KS orbitals are generated, one for the α-spin electrons, *i.e.,* the “spin-up” ones, and one for the β-spin electrons, *i.e.,* the “spin-down” ones).

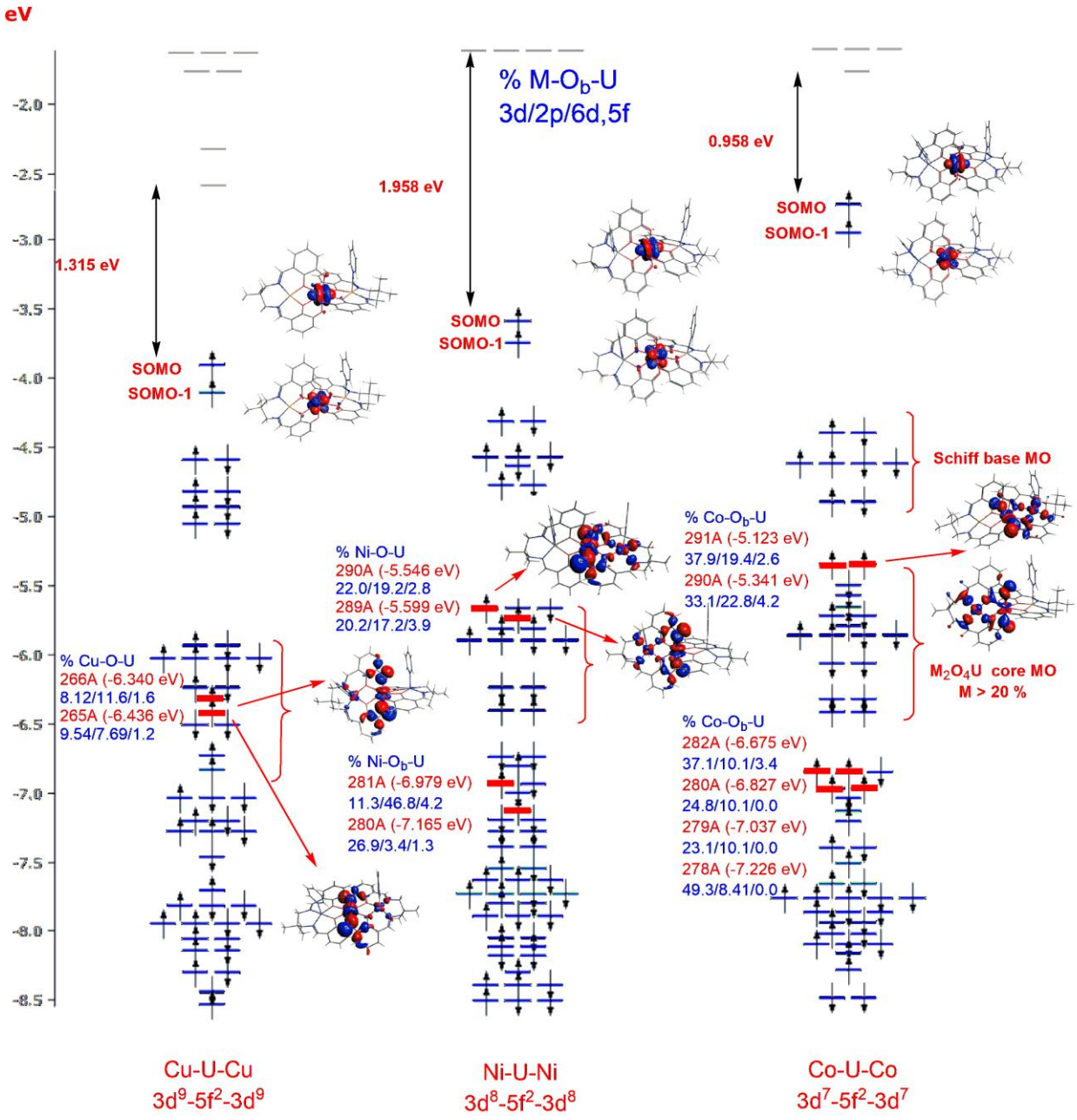

Figure 4: ZORA/B3LYP HS KS spin orbital diagrams of the MUM (Cu, Ni, Co) complexes

One can note in these diagrams that the highest levels composed of the SOMO and SOMO-1 with the two pure metallic α singly $5f^2$, appear slightly more destabilized in the Ni_2U and Co_2U systems than in the Cu_2U cases. Notably, the spin orbitals displaying the two $Cu(3d^9)$–$Cu(3d^9)$, four $Ni(3d^8)$ –$Ni(3d^8)$, and six $Co(3d^7)$–$Co(3d^7)$ metallic electrons, as shown by their isodensity surfaces, are highly delocalized and deeper in energy relatively to the SOMO/SOMO-1 ($5f^2$).

In Table 3 are reported the computed compositions % and energy of the SOMOs and the most relevant M_2O_4U (Cu, Ni, Co) MO magnetic core and displaying the M–O_b–U bridging bonding in term of % of M(3d)/O(2p)/U(6d,5f) orbitals.

Table 3: ZORA/B3LYP/TZP percentages orbital compositions of the M_2O_4U (Cu, Ni, Co) MO magnetic cores

MUML fixed core	M--U (Å)	Energy (eV) % (U(5f) / M(3d) / O(2p))			
		SOMO	SOMO-1	SOMO#	
CuUCu	3.634/3.648	–3.902 90.7/0/0	–4.106 74.0/0/6.1	SO-18 (–6.340) 19.54/7.69/1.2	SO-19 (–6.436) 8.12/11.6/1.6
NiUNi	3.633/3.652	–3.584 92.3/0/0	–3.750 92.6/0/0	SO-12 (–5.546) 20.2/17.2/3.9	SO-14 (–5.599) 22.0/19.2/2.6
CoUCo	3.666/3.693	–2.746 91.4/0/0	–2.953 94.2/0/6.3	SO-10 (–5.123) 33.1/22.8/4.2	SO-11 (–5.341) 37.9/19.4/2.6

Interestingly, the orbital (% 3d/2p/6d,5f) composition of the SOMO-12/-14 (#289/#290) and SOMO-10/-11 (#290/#291) in the Ni_2UL and Co_2UL systems, respectively (Figure 4), traducing the M-O_b-U bridging bonds, is computed to display higher metallic/oxo contributions in the Ni_2UL and Co_2UL systems (% 20.2/17.2/3.9 and 22.0/19.2/2.6 vs. % 33.1/22.8/4.2 and 37.9/19.4/2.6) than the SOMO-18/-19 (#265/#266) with % 19.54/7.69/1.2 and 8.12/11.6/1.6 in the Cu_2UL congener. These results sustain the more pronounced covalent character of the Ni-O_b–U and Co-O_b–U bridging bonds than in their Cu-O_b–U congeners already revealed by the bond orders.

The electronic structure analysis of the MO diagrams shows that the superexchange M–O–U coupling likely involves the 6d/5f orbitals of the U^{IV} ion (mainly dz^2, dx^2-y^2, f_{xyz}, f_{zy}^2, f_{zx}^2) that have the appropriate energy and symmetry matching to overlap with the oxo-(2p) and the magnetic transition metal 3d ($3d_{x^2-y^2}$) orbitals centered on each Cu^{II} ion (Figure 4)".

Moreover, the MO analysis of the Co_2UL and Ni_2UL systems, exhibit larger (6d, 5f) uranium weight in M_2O_4U magnetic core than in their Cu_2UL congener.

These features were previously observed with the trinuclear Cu_2UL^i (i = 1-9) systems, exhibiting AF/Ferro switch with the elongation of Cu—U distance, bringing to light the crucial influence of the orbital contribution to the Cu—O_b—U bridging bonding on the magnetic character [35].

Finally, the MO analysis corroborates the BO results (Table 2) regarding the more pronounced covalent factors of the M–O_b–U bridging bonds in the Ni_2UL and Co_2UL comparatively to the Cu_2UL congener, which likely explain the difference in their AF vs. Ferro superexchange M–U–M interactions.

c. Magnetic properties

Evaluation of the coupling constant J (cm^{-1})

As shown on Scheme 2, we first investigate the different spin couplings in the systems under consideration. Indeed, it was shown for the trinuclear Cu^{II}–U^{IV}–Cu^{II} (S_{Cu} = ½, S_U = 1) system [35] that the ideal $<S^2>$ values were 6 for the HS solution, 2 for BS and 3 for BS1 and BS2 ones. Those values correspond to the perfect Ising case, for which the spin contamination exactly corresponds to the one that would be observed at dissociation, *i.e.* in the absence of coupling. The genuine strategy to sort out those ideal values consists in generating appropriate spin functions that are eigenfunctions of the $<S^2>$ operator, and in attributing the character of the spin determinants of interest in terms of pure spin functions. For instance, since the HS solution is there of pure S = 2 character, the ideal $<S^2>$ value for this solution corresponds to the one of a pure S = 2 state, *i.e.,* S(S+1) = 2*3 = 6.

In the case of a trinuclear Ni^{II}–U^{IV}–Ni^{II} core, *i.e.,* for the coupling of S_a = 1 with S_b = 1 and S_c = 1, one may use tabulated values from the literature [66] to determine the ideal $<S^2>$ values. First, let us recall that in this case, a simple spin tree approach based on successive couplings may help in defining the space of the HDvV Hamiltonian: the coupling of two local S_a = 1 and S_b = 1 spins generates one S_{ab} = 2, one S_{ab} = 1 and one S_{ab} = 0 states, and the coupling of those with a third S_c = 1 spin then generates one S = 3 state (with S_{ab} = 2), two S = 2 states (with S_{ab} = 2 or S_{ab} = 1), three S = 1 states (with S_{ab} = 2, S_{ab} = 1 or S_{ab} = 0) and one S = 0 state (with S_{ab} = 1). Of course, the HS solution is trivial, it corresponds to the S = 3 state and thus to an ideal $<S^2>$ value of 3*4 = 12. The remaining BS, BS1 and BS2 solutions all correspond to $|M_S|$= 1, and their spin nature is in fact identical [66]: these correspond to 1/15 of S = 3 character, 1/3 of S = 2 character, and 3/5 of S = 1 character. Consequently, their ideal $<S^2>$ values are 1/15*3*4+1/3*2*3+3/5*1*2 = 4.

Finally, we now need the ideal $<S^2>$ values corresponding to the trinuclear $Co^{II}–U^{IV}–Co^{II}$ situation, *i.e.,* to the $S_a = 3/2$ with $S_b = 1$ and $S_c = 3/2$ case. By applying the same methodology, one can justify the space of the HDvV Hamiltonian: one $S = 4$ state (with $S_{ab} = 5/2$), two $S = 3$ states (with $S_{ab} = 5/2$ or $S_{ab} = 3/2$), three $S = 2$ states (with $S_{ab} = 5/2$, $S_{ab} = 3/2$ or $S_{ab} = 1/2$), three $S = 1$ states (still with $S_{ab} = 5/2$, $S_{ab} = 3/2$ or $S_{ab} = 1/2$) and one $S = 0$ state (with $S_{ab} = 3/2$). The HS solution ideally being of pure $S = 4$ character, its ideal $<S^2>$ value is trivially 4*5 = 20. The BS solution corresponding to the $|M_S| = 2$ subspace, it may bear some $S = 4$, $S = 3$ and $S = 2$ characters. After some development, we found that it corresponds to 1/28 of $S = 4$, 1/4 of $S = 3$ and 5/7 of $S = 1$ characters, leading to an ideal $<S^2>$ value of 1/28*4*5+1/4*3*4+5/7*3*2 = 8. The BS1 and BS2 solutions both belong to the $|M_S| = 2$ subspace, meaning that those may now bear some $S = 4$, $S = 3$, $S = 2$ and $S = 1$ characters. After having shown that the respective weights are 1/56, 1/8, 5/14 and 1/2, we obtain ideal $<S^2>$ values of 1/56*4*5+1/8*3*4+5/14*2*3+1/2*1*2 = 5.

Experimentally, the variable-temperature measurements of the Cu_2UL, Ni_2UL, and Co_2UL systems show distinct superexchange interactions between the magnetic metals within the M_2O_4U magnetic core [24, 31-34]. The bicentric Cu–U spin carriers, as previously described [34-36], are ferromagnetically coupled, whereas the Ni–U coordination exhibit AF interactions. To get more insights into such differences between these magnetic characters, the magnetic coupling constants J (cm^{-1}) have been computed using the HS/BS approach with equations 6-8 for the Ni-U-Ni system, and 13,17,18 for the Co-U-Co analogous (*vide supra*). The considered Co_2UL and Ni_2UL[7] systems feature the $3d^7–5f^2–3d^7$ and $3d^8–5f^2–3d^8$ valence electron configurations, respectively.

In Table 4, are reported the energy (TBE) of the high spin (HS) and BS spin states, the BS1 and BS2, a mixing of lower spin states, as well as the ideal values of the $<S^2>$ operators. The calculations have been carried out by fixing the magnetic core as it is in the X-ray structure.

Table 4: Computed TBE for the HS, BS, BS1 and BS2 states (in eV), together with the corresponding $\langle S^2 \rangle$ values.

MUML (eV) RX-fc	HS	BS	BS1	BS2	$\langle S^2 \rangle$ (ideal)			
					HS	BS	BS1	BS2
NiUNi ($S_{max} = 3$)	−806.0263	−806.0265	−806.0266	−806.0266	12.01 (12)	4.02 (4)	4.02 (4)	4.01 (4)
CoUCo ($S_{max} = 4$)	−839.7951	−839.7968	−839.7964	−839.7966	20.04 (20)	8.01 (8)	5.03 (5)	5.03 (5)

Table 4 shows that for the HS states, the $\langle S^2 \rangle$ spin contamination is negligible for a pure septet (NiUNi) and nonet (CoUCo) spin states, comparatively to the ideal values i.e., $\langle S^2 \rangle_{ideal}$ = 12 and 20, respectively. Of course, the BS, BS1 and BS2 solutions do not correspond to the exact values for pure spin states, but rather to the ideal ones derived above (4, 8 and 5 at the appropriate places in Table 4).

The computed exchange coupling constants J_{12} and J_{23} for adjacent M1−U and M2−U metals, and J_{13} constant for next-adjacent M1−M3 (Ni, Co) atoms are reported in Table 5.

Table 5: Computed ZORA/B3LYP/TZP exchange coupling J_{12}, J_{23}, J_{13} (cm^{-1}) as well as the average $J_{M\text{-}U}$ constants $J_{M\text{-}U} = (J_{12} + J_{23})/2$ for the Ni_2UL and Co_2UL X-ray structures compared to the Cu_2UL values.

MUML[7] RX-fc	M---U (Å)	<M-O-U> (°)	J_{12}	J_{23}	J_{13}	$J_{M\text{-}U}$
Cu_2UL (S =2)	3.634/3.648	111.5/112.3	2.31	1.15	–0.29	+1.73[a]
Ni_2UL (S = 3)	3.633/3.652	110.6/111.7	–1.37	–1.44	–0.38	–1.41
Co_2UL (S = 4)	3.666/3.693	110.4/111.3	–2.11	–2.65	–0.94	–2.38

[a] *ref. [35]*

As previously noted [35], the results (Table 5) show that the two exchange couplings J_{12} and J_{23} (cm^{-1}) for adjacent M1−U and M2−U metals are different due to the coordination environmental effects around the two M(II) (Ni, Co) centers. Notably, as shown in Table 5 comparing the Ni_2UL and Co_2UL systems to their Cu_2UL congener, beyond the computed $J_{M\text{-}U}$ reproduce correctly the AF and Ferro character, respectively, the computed coupling constants ($-2.38 < J < +1.73$ cm^{-1}) fit fairly well the experimental fitted ones ($-3.6 < J_{min} < +5.2$ cm^{-1}) for the mixed 3d-5f complexes with available X-ray Cu_2UL[1-9] structures [24].

Considering the computed exchange J_{13} constant, the M1−M2 (Ni, Co) coupling appears weak which agrees well with the experimental trends [24, 31-34]. These results match well with the observed weak intramolecular AF or no-interacting Ferro M1−M2 coupling, as pointed out by the susceptibility measurements of the M_2UL (M = Co, Ni, Cu) systems [32-34].

Furthermore, the influence of the coordination environment of the metals on the magnetic properties is explored by considering the mixed $Zn^{II}U^{IV}M^{II}L$ and $M^{II}_2Th^{IV}L$ model systems, where one M^{II} (Co = $3d^7$, Ni = $3d^8$) as well as the U^{IV} ($5f^2$) paramagnetic centers, are replaced by diamagnetic Zn^{II} ($3d^{10}$) and Th^{IV} ($5f^0$) ones, respectively. Such investigations have been successfully used in the case of the trimetallic Cu_2UL^i model systems [35], revealing the effects of coordination properties of transition metal variation on the strength and nature of the two sides of magnetic M^{II}–U^{IV}–M^{II} couplings.. Starting from the available X-ray Zn_2AnL structures [32-34] two $Zn^{II}U^{IV}M^{II}L$ and $M^{II}_2Th^{IV}L$ (M = Co, Ni) models have been optimized and their HS/BS energies computed keeping one side M–U distance fixed to its available X-ray value, regarding the two Zn–U/M1–U and M2–U/Zn–U ones [33,34]. The other Zn–U side distance, in opposite, is optimized in their HS quintet (S = 2) and sextet (S = 5/2) for the two $Zn^{II}U^{IV}M^{II}L$ (M = Ni, Co) models, respectively. The coupling J_{M-U} constants, are computed for the HS/BS states using the Yamaguchi formula (*vide supra*). The optimized parameters *i.e.,* M–U (Å) intermetallic distances, <M–O–U> (°) bond angles, HS/BS energy (TBE) and the corresponding $<S^2>$ values, as well as the coupling J_{M-U} constants are reported for the two MUZn and MThM models in Table 6.

Table 6: Computed TBE for the HS/BS states of the mixed MAnZn (M = Co, Ni; An = Th, U) model complexes, energy difference $\Delta E = E_{BS} - E_{HS}$ (eV), $\langle S^2 \rangle_{HS/BS}$ values (exact values of are given between parentheses for comparison) and exchange magnetic coupling constant J_{M-U} (cm^{-1}).

MAnM'	S_{max}	M---U (Å)	<M-O-U> (°)	HS	BS	⟨S⟩² (ideal)		J_{MU} (cm^{-1})
						HS	BS	
NiUZn	2	3.633/3.792	110.5/112.6	–823.8031	–823.8058	6.01 (6)	2.01 (2)	–5.44
ZnUNi	2	3.777/3.652	113.0/110.9	–823.7822	–823.7850	6.01 (6)	2.01 (2)	–5.64
NiThNi	2	3.789/3.795	112.0/112.2	–826.1816	–826.1817	6.01 (6)	2.01 (2)	–0.20
CoUZn	5/2	3.693/3.780	111.6/112.2	–828.3065	–828.3100	8.77 (8.75)	2.75 (2.75)	–3.61
ZnUCo	5/2	3.785/3.666	112.5/110.4	–828.3107	–828.0893	8.77 (8.75)	2.76 (2.75)	–1.07
CoThCo	3	3.799/3.787	111.9/111.7	–835.3565	–835.3566	12.03 (12)	3.03 (3)	–0.07

From Table 6, the computed coupling constants for the mixed ZnUM species, using the Yamagushi formula [55-57], confirm the AF character of the M^{II}–U^{IV} exchange interactions. The BS solutions do not correspond to pure spin states but rather to ideal mixtures ($<S^2>$ ideally

being 2 and 2.75, respectively). Concerning the MThM complexes, starting from the X-ray M_2ThL (M = Ni, Co) structure derivatives [32,33], the calculations were carried out taking into account the HS triplet state $3d^{\alpha\alpha}–5f^0–3d^{\alpha\alpha}$ (M_S = 2) for NiThNi systems, and $3d^{\alpha\alpha\alpha}–5f^0–3d^{\alpha\alpha\alpha}$ (M_S = 3) for CoThCo congener. The BS $3d^{\alpha\alpha}–5f^0–3d^{\beta\beta}$ (M_S = 0) and $3d^{\alpha\alpha\alpha}–5f^0–3d^{\beta\beta\beta}$ (M_S = 0) configurations, are considered, respectively. These solutions match the expected $<S^2>$ values (2 and 3, respectively).

The results of Table 6 show that M---M non-adjacent spin carriers, are weakly coupled, as shown by their $J_{M—M}$ NiThNi (–0.20 cm^{-1}), and CoThCo (–0.07 cm^{-1}). These theoretical results (Table 6) are consistent with the reported fitted magnetic susceptibility data of X-ray thorium Cu_2ThL^i (i = 1, 2) [32, 33], using the HDvV isotropic spin Hamiltonian $H = –JS_{Cu1}\cdot S_{Cu2}$, with $S_{Cu1} = S_{Cu2} = ½$, led to the values of $J_{Cu\text{-}Cu}$ = –0.84 and –0.48 cm^{-1} for the Cu_2ThL^1 and Cu_2ThL^2, respectively. In contrast, it was found that for the analogous Cu_2ThL^7 system, the two Cu---Cu ($3d^9$---$3d^9$) ions are non-interacting or weakly ferromagnetically coupled [32-34].

Spin Density Analysis.

For a qualitative understanding of ferromagnetic and AF exchange coupling, the mapping of spin densities, revealed crucial to explain the exchange coupling between the magnetic centers in d-transition metal magneto-chemistry [67, 68]. Indeed, some mechanisms have been proposed including spin polarization, spin delocalization, or superexchange as outlined in the early 1990s by O. Kahn [69]. Table 8 presents the obtained HS/BS natural spin density distributions (difference between α and β electron densities) for the three M_2UL (M = Cu, Ni, Co) complexes with fixed M_2O_4U core.

Table 8: ZORA/B3LYP/TZP NPA spin populations for the HS and BS states of M_2UL (M = Cu, Ni, Co) with X-ray fixed core. Atoms are numbered as indicated on Figure 3.

M_2UL	Cu_2UL		Ni_2UL		Co_2UL	
Atoms	HS	BS	HS	BS	HS	BS
U	2.042	2.033	2.036	2.032	2.044	2.037
M_1	0.637	–0.633	1.611	–1.413	2.628	–1.904
M_2	0.609	–0.605	1.616	–1.507	2.623	–1.908
O_{b1}	0.080	–0.081	0.067	–0.049	0.077	–0.022
O_{b2}	0.081	–0.081	0.070	–0.052	0.079	–0.011
O_{b3}	0.088	–0.089	0.071	–0.059	0.079	–0.024
O_{b4}	0.087	–0.088	0.068	–0.053	0.081	–0.022

One can note that both HS and BS states exhibit well-localized spin densities on the uranium(IV) center, while the bridged d-metal ions i.e., $Cu^{II}(3d^9)$, $Ni^{II}(3d^8)$, and $Co^{II}(3d^7)$, exhibit significantly lower spin densities than formal polarization values, i.e., 1, 2, and 3, respectively. Oxidation and spin delocalization effects likely explain this phenomenon, corroborating well the pictured MO and electronic structure analysis, over the bridged M_2O_4U magnetic core.

On Figure 5 are shown the spin mapping of the HS, BS, BS1, and BS2 states. Interestingly, the spin density maps along the path linking the M_2O_4U magnetic core, show non-negligible values for the oxo-bridging atoms which contribute to the exchange coupling mechanism, as shown by Figure 5 depicting spin densities mapping.

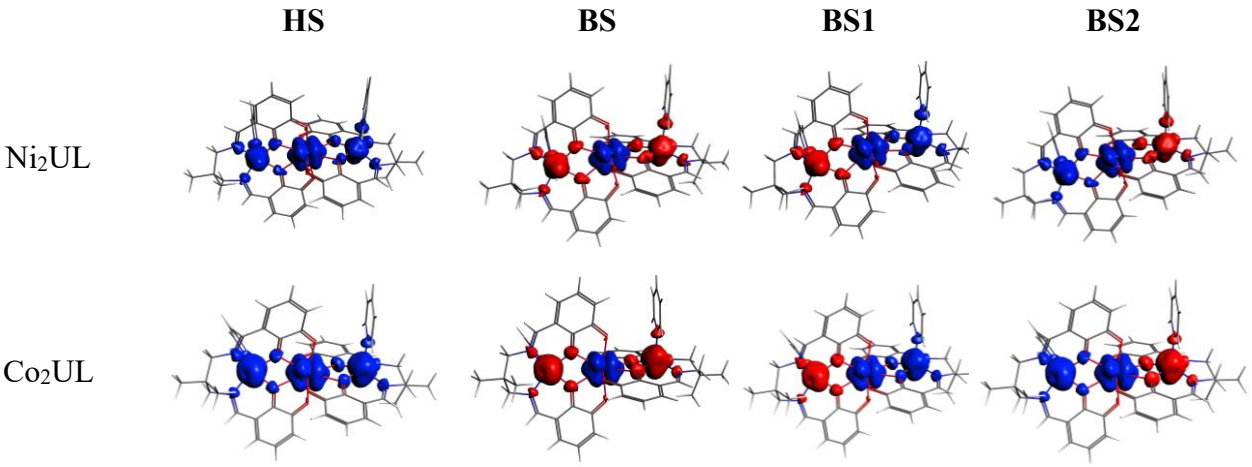

Figure 5: Mapping representations of the ZORA/B3LYP/TZP spin densities for the HS, BS, BS1, and BS2 spin states of the M_2UL (M = Ni, Co) complexes (blue color: positive and red color: negative spin density). The isodensity surface corresponds to a value of 0.004 e $bohr^{-3}$.

It is worth noting that for the Cu_2UL Ferro system, the spin densities of the two metal Cu(II) centers remain unchanged when passing from the HS to the BS solutions, while for the M_2UL (Ni, Co) AF congeners, the spin densities of metal centers decrease significantly from the HS to the BS state, especially for the Co_2UL system. This is also true for the oxo-bridging atoms, where spin densities decrease drastically from the HS to the BS state. This is likely to highlight the crucial spin delocalization role of the bridging M_2O_4U core favoring antiferromagnetic coupling of the M_2UL (Ni, Co) complex, in opposite to the Ferro Cu_2UL congener.

Specific discussion to the CoUCo complex

Though the nature of the coupling is clear in the Cu_2UL (Ferro) and Ni_2UL (AF) cases, it is worth commenting on more deeply on the Co_2UL one. As previously mentioned, the $\Delta\chi_M T$ vs

T curve behaves exactly the same as the one observed in the Ni_2UL case. However, transferring the same reasoning on the Co_2UL case requires the angular momentum on the Co^{II} centers to be significantly quenched by the local coordination environment. We would like to stress that our DFT calculations have predicted an AF coupling between the Co^{II} ions and the U^{IV} one, and that this fact alone could explain the observed trend (continuous increase in the $\Delta\chi_M$T vs *T* curve even well above 100 K). As stated by the authors in the original experimental publication [32], the Co^{II} ions are in a tetragonally distorted environment. Depending on the magnitude of the distortion, it may ultimately lead to a fully quenched orbital momentum. Recently, in a less distorted situation, some of us have showed that even a moderate distortion of the octahedral arrangement may lead the local anisotropy occurring in the Co^{II} center to be consistently mapped into a simple zero-field splitting Hamiltonian, with local anisotropy parameters *D*'s of the order of 100 cm^{-1} [38]. By accounting for the SOC in the calculations and using sophisticated models including isotropic and anisotropic exchange plus simulating the χ_MT vs *T* curves, we have shown that only AF coupling could explain a continuous increase (Ferro coupling in conjunction with axial local anisotropy leading to a local maximum at low temperature). We would also like to point out that increase in the number of magnetic orbitals in the peripherical transition metals potentially opens the way for more kinetic exchange and superexchange pathways, thus there should be more and more tendency to display AF coupling by going from Cu_2UL to Ni_2UL to Co_2UL. Furthermore, in all those systems, structure is key to explain the magnetism, and the key angular parameter, *i.e.* the <M–O_b–M> bond angle, is practically the same in both the Ni_2UL and Co_2UL cases. For all those reasons, we are quite confident in our predicted nature of the coupling in the Co_2UL case, which is AF. Naturally, a full elucidation of the magnetism in this system would require a full study that also include the SOC, which is out of the scope of the present work.

We would just like to stress that in previous studies that have determined the magnitude of the isotropic coupling between two close Cu^{II}, Ni^{II}, or Co^{II} paramagnetic centers with and without the SOC [38, 70, 71], only a minor effect of the SOC on the extracted coupling constant was observed (typically it is reduced by 1–10%), but that in our experience, the SOC has never turned out to change the *J* sign, which again justifies our present approach to predicting the nature of the coupling (Ferro or AF).

Conclusion:

In summary, the exchange coupling constants of the M–U in a series of isostructural trinuclear Schiff base bridged (M^{II} = Co, Ni, Cu, L = Schiff base) complexes have been investigated theoretically using scalar relativistic DFT computations (without spin-orbit coupling effects) at the ZORA/B3LYP/TZP level, combined with the broken symmetry (BS) approach.

Such studies on mixed 3d–5f compounds are crucial because of their importance in the fundamental understanding of the nature of metal–ligand bonding and metal–metal electronic interactions between 3d and 5f elements. The considered M_2UL (Cu, Co, Ni) complexes exhibit similar M(II)-O_b-U(IV) oxo-bridged coordination but different magnetic behavior regarding the M–U exchange coupling. The main significant structural differences regarding the M(μ-O_b)$_2$U magnetic core are the M–O_b–U angles or the M–U distance when changing the transition metal. The electronic structure analysis of bond orders shows that the more pronounced covalent factors of the M–O_b and U–O_b bonds in the Ni_2UL and Co_2UL, in comparison with the Cu_2UL congener, are playing a significant role in promoting M–U–M superexchange AF interactions. These results are sustained by the MO analysis, which shows that the 6d/5f orbitals are effectively involved in the AF superexchange M–U–M (Ni, Co) coupling, contributing more significantly than in the cases of the Ferro Cu–U–Cu one. Notably, comparing the Ni–U–Ni system to the Cu–U–Cu congener, the computed $J_{M\text{-}U}$ (–1.41 vs. +1.73 cm^{-1}) reproduces correctly the weak AF vs. Ferro character of these two complexes, in good agreement with the available experimentally fitted values. We also predict a small AF coupling in the Co_2UL system (–2.38 cm^{-1}), which is consistent with the experimental data and that we have further justified by several qualitative arguments.

Supplementary Information

-Optimized coordinates

Supplementary data to this article can be found online.

AUTHOR INFORMATION

Corresponding Authors

Abdou Boucekkine − Univ Rennes, ISCR UMR 6226 CNRS

Campus de Beaulieu, 35042 Rennes Cedex, France.

https://orcid.org/0000-0002-3714-7191

Email: abdou.boucekkine@univ-rennes1.fr

Lotfi Belkhiri − Laboratoire de Physique Mathématique et Subatomique LPMS

Département de Chimie, Université des Frères Mentouri Constantine 1

Route Ain El Bey 25017, Constantine, Algeria.

https://orcid.org/0000-0002-6093-6965

Email: lotfi.belkhiri@umc.edu.dz

Acknowledgments

The authors are grateful to the Frères Mentouri University of Constantine 1 (Algeria) and the Pharmaceutical Sciences Research Center (CRSP) for providing computing facilities. The General Directorate of Scientific Research and Technological Development (DGRSDT) for the PRFU project (2022-2024: Grant No. B00L01EN250120220001) and the Thematic Research Agency in Health and Life Sciences – ATRSSV for the PNR (Grant 2022-2024) are also acknowledged. The French GENCI IDRIS and GENCI-CINES are acknowledged for an allocation of computing time (Grant No. 2022-080649).

References:

1. M. Liu, X.-H. Peng, F.-S. Guo, M.-L. Tong, *Inorg. Chem. Front*., **2023**, *10*, 3742-3755.
2. S. Dey, G. Rajaraman, H.Bolvin, *Chemistry - A European Journal*, **2022**, *28(68),* e202201883.
3. L. Belkhiri, B. Le Guennic, A.Boucekkine, *Magnetochemistry* **2019**, *5*, 15.
4. C. Camp, D. Toniolo, J. Andrez, J. Pécauta, M. Mazzanti, *Dalton Trans*., **2017**, *46*, 11145-11148.
5. J. R. Long, K. R. Meihaus, *Dalton Trans*. **2015**, *44*, 2517–2528.
6. S. T. Liddle, *Angew. Chem. Int. Ed.* **2015**, *54*, 8604–8641.
7. N. Magnani, *Int. J. Quantum Chem*. **2014**, *114*, 755–759.
8. S.T. Liddle, J. van Slageren, Lanthanides and Actinides. In Molecular Magnetism Layfield, R.A., Murugesu, M., Eds. Wiley-VCH: Weinheim, Germany, **2015** pp. 315–340.
9. R. A. Layfield, Organometallics, **2014**, *33*, 1084–1099.
10. S.G. McAdams, A-M. Ariciu, A.K. Kostopoulos, J.P.S. Walsh, F. Tuna, *Coord. Chem. Rev*. **2017**, *346*, 216-239,
11. S.T. Liddle, J. van Slageren, *Chem. Soc. Rev*. **2015**, *44*, 6655–6668.
12. L. Chatelain, F. Tuna, J. Pécaut, M. Mazzanti. *Dalton Trans*., **2017**, *46*, 5498-5502.
13. L. Chatelain, J. Pécaut, F. Tuna, M. Mazzanti, *Chem. – Eur. J.,* **2015**, *21(50*), 18038-18042.
14. L. Chatelain, J.P.S. Walsh, J. Pécaut, F. Tuna, M. Mazzanti, *Angew. Chem., Int. Ed.* **2014**, *53(49*), 13434-13438.

15. V. Mougel, L. Chatelain, J. Pécaut, R. Caciuffo, E. Colineau, J.-C. Griveau, M. Mazzanti, *Nat. Chem*., **2012**, *4*, 1011–1017.
16. E. Ruiz, J. Cano, S. Alvarez, P. Alemany, *J. Comput. Chem*. **1999**, *20*, 1391-1400.
17. Ruiz, E. Theoretical Study of the Exchange Coupling in Large Polynuclear Transition Metal Complexes Using DFT Methods. In: Principles and Applications of Density Functional Theory in Inorganic Chemistry II. Structure and Bonding, vol 113. Springer, Berlin, Heidelberg, **2004**.
18. F. Neese, *Coord. Chem. Rev*. **2009**, *253*, 526-563.
19. G. David, F. Wennmohs, F. Neese, N. Ferré, *Inorg. Chem*. **2018**, 57, 12769-12776.
20. X. Sheng, L. M. Thompson, H. P. Hratchian, *J. Chem. Theory Comput*. **2020**, *16*, 154−163.
21. I. Rudra, Q. Wu, T.Van Voorhis, *Inorg. Chem*. **2007**, 46, 10539−10548.
22. W.W. Lukens, M. Speldrich, P. Yang, T.J. Duignan, J. Autschbach, P. Kögerler, *Dalton Trans*. **2016**, *45*, 11508–11521.
23. D. Reta, F. Ortu, S. Randall D. P. Mills, N. F. Chilton, R. E. P. Winpenny, L. Natrajan, B. Edwards, N. Kaltsoyannis, *J. Organomet. Chem.* **2018**, *857*, 58–74.
24. J. D. Rinehart, T.D. Harris, S.A. Kozimor, B.M. Bartlett, J.R. Long, *Inorg. Chem.*, **2009**, *48*, 3382-3395.
25. S. Boucenina, L. Belkhiri, S. Meskaldji, R. Linguerri, G. Chambaud, A. Boucekkine, M. Hochlaf. *J. Mol. Model*. **2020**, *26*, 282.
26. B. Teyar, S. Boucenina, L. Belkhiri, B. Le Guennic, A. Boucekkine, M. Mazzanti. *Inorg. Chem*. **2019**, *58*, 10097-10110.
27. S. Meskaldji, A. Belkhiri, L. Belkhiri, A. Boucekkine, M. Ephritikhine, *C R. Chimie* **2012**, *15*, 184-191.
28. L. P. Spencer, E. J. Schelter, P. Yang, R. L. Gdula, B. L. Scott, J. D. Thompson, J. L. Kiplinger, E. R. Batista, J. M. Boncella, *Angew. Chem. Int. Ed.* **2009**, *48*, 3795–3798.
29. B. S. Newell, A. K. Rapp, M. P. Shores, *Inorg. Chem*. **2010**, *49*, 1595–1606.
30. S. Hohloch, J.R. Pankhurst, E.E. Jaekel, B.F. Parker, D.J. Lussier, M.E. Garner, C.H. Booth, J.B. Love, J. Arnold, *Dalton Trans*. **2017**, *46*, 11615–11625.
31. T. Le Borgne, E. Riviere, J. Marrot, J. J. Girerd, M. Ephritikhine, *Angew. Chem., Int. Ed.*, **2000**, *39*, 1647–1649.
32. L. Salmon, P. Thuéry, E. Rivière, J. Marrot, J.-J. Girerd, M. Ephritikhine, *Chem. Eur. J.* **2002**, *8*,773–783.
33. L. Salmon, P. Thuéry, E. Rivière, J.-J. Girerd, M. Ephritikhine, *Dalton Trans*. **2003**, 2872–2880.
34. L. Salmon, P. Thuéry, E. Rivière, J.-J. Girerd, M. Ephritikhine, *Inorg. Chem*. **2006**, *45*, 83–93.
35. S. Meskaldji, L. Belkhiri, R. Maurice K. Costuas B. Le Guennic, A. Boucekkine, M. Ephritikhine, J. *Phys. Chem. A* **2023**, *127*, 6, 1475–1490.
36. S.A. Kozimor, B.M. Bartlett, J.D. Rinehart, J.R. Long, *J. Am. Chem. Soc*. **2007**, *129*, 10672–10674.
37. J. D. Rinehart, B. M. Bartlett, S. A. Kozimor, J. R. Long, *Inorg. Chim. Acta* **2008**, *361*, 3534–3538.
38. D.-C. Sergentu, B. Le Guennic, R. Maurice, *Phys. Chem. Chem. Phys*. **2024**. (Advance Article)

39. G. te Velde, F. M. Bickelhaupt, E. J. Baerends, C. Fonseca Guerra, S. J. A. van Gisbergen, , J. G. Snijder, T. Ziegler, *J. Comput. Chem.* **2001**, *22*, 931-967.
40. R. Rüger, M. Franchini, T. Trnka, A. Yakovlev, E. van Lenthe, P. Philipsen, T. van Vuren, B. Klumpers, T. Soini. Amsterdam Modeling Suite (AMS version: 2021.107), Software for Chemistry & Materials SCM, Theoretical Chemistry, Vrije Universiteit, Amsterdam, The Netherlands, http://www.scm.com
41. E. van Lenthe, E. J. Baerends, J. G. Snijders, *J. Chem. Phys*. **1993**, *99*, 4597-4610.
42. E. van Lenthe, A. E. Ehlers, E. J. Baerends, *J. Chem. Phys*. **1999**, *110*, 8943-8953.
43. A. Døssing, *Coord. Chem. Rev*. **2014**, *280*, 38−53.
44. S. Ouilia, C. Beghidja, A. Beghidja, L. Belkhiri, P.Rabu, *Inorg. Chim. Acta* **2018**, *476*, 54−60.
45. Becke, A. D. *Phys. Rev. A*, **1988**, *38*, 3098−3100.
46. J. P. Perdew, *Phys. Rev. B*, **1986**, *33*, 8822−8824.
47. A. J. Gaunt, S. D. Reilly, A. E. Enriquez, B. L. J. A. Scott, Ibers, P. Sekar, K. I. M. Ingram, N. Kaltsoyannis, M. P. Neu, *Inorg. Chem*. **2008**, *47*, 29−41.
48. C. R. Graves, P. Yang, S. A. Kozimor, A. E. Vaughn, D. L. Clark, S. D. Conradson, E. J. Schelter, B. L. Scott, J. D. Thompson, P. J. Hay D. E. Morris, J. L. Kiplinger, *J. Am. Chem. Soc*. **2008**, *130*, 5272–5285.
49. A. D. Becke, *J. Chem. Phys*. **1993**, *98*, 5648.
50. C. Lee, W. Yang, R. G. Parr, *Phys. Rev. B* **1988**, *37*, 785.
51. J. E. Peralta, J. I. Melo, *J. Chem. Theory Comput*. **2010**, *6*, 1894−1899.
52. L.J. Noodleman, E. R. Davidson, *J. Chem. Phys*. **1986**, *109*, 131–143.
53. L. J. Noodleman, C. Y. Peng, D. A. Case, J. M. Mouesca, *Coord. Chem. Rev*. **1995**, *144*, 199–244.
54. S. K. Singh, N. K. Tibrewal, G. Rajaraman. *Dalton Trans*., **2011**, *40*, 10897.
55. K. Yamaguchi, F. Jensen, A. Dorigo, K.N. Houk, *Chem. Phys. Lett*. **1988**, *149*, 537.
56. T. Onishi, D. Yamaki, K. Yamaguchi, Y. Takano, *J. Chem. Phys*. **2003**, *118*, 9747−9761.
57. M. Shoji, K. Koizumi, Y. Kitagawa, T. Kawakami, S. Yamanaka, M. Okumura, K. Yamaguchi, Chem. Phys. Lett. **2006**, *432*, 343−347.
58. I. Ciofini, C.A. Daul, *Coord. Chem. Rev*. **2003**, *187*, 238.
59. A.E. Reed, L. A. Curtiss, F. Weinhold, *Chem. Rev*. **1988**, *88*, 899.
60. I. Mayer, Charge, *Chem. Phys. Lett*. **1983**, *97*, 270.
61. R. F. Nalewajski, J. Mrozek, *Int. J. Quantum Chem*. **1994**, *51*, 187.
62. R.F. Nalewajski, J. Mrozek A. Michalak, *Int. J. Quantum Chem*. **1997**, *61*, 589.
63. A. Døssing, *Coord. Chem. Rev*. **2014**, *280*, 38−53.
64. T. J. Morsing, J. Bendix, H. Weihe, A. Døssing. *Inorg. Chem*. **2014**, *53*, 6, 2996
65. P. J Hay, J C. Thibeault, R. Hoffmann, *J. Am. Chem. Soc*. **1975**, *97(17)*, 4884–4899
66. J.-M. Lévy-Leblond, M. Lévy-Nahas, *J. Math. Phys*. **1965**, *6*, 1372–1380.
67. F. Neese, *Coord. Chem. Rev*. **2009**, *253*, 526−56.
68. J. Cirera, Y. Jiang, L. Qin, Y.-Z. Zheng, G. Li, G. Wu, E. Ruz, *Inorg. Chem. Fron*t. **2016**, *3*, 1272-1279.
69. O. Kahn, Molecular magnetism VCH: New York, **1993**.
70. R. Maurice, A. M. Pradipto, N. Guihéry, R. Broer, C. de Graaf, *J. Chem. Theory Comput*. **2010**, *6(10)*, 3092–3101.
71. R. Maurice, N. Guihéry, R. Bastardis, C. de Graaf. *J. Chem. Theory Comput*. **2010**, *6(1)*, 55–65.